

EFFECT OF SAMPLING IN CREATING A DIGITAL IMAGE ON MEASUREMENT ACCURACY OF CENTER LOCATION OF A CIRCLE

R. Matsuoka^{a,b,*}, M. Sone^a, N. Sudo^a, H. Yokotsuka^a, N. Shirai^b

^a Tokai University Research & Information Center, 2-28-4 Tomigaya, Shibuya-ku, Tokyo 151-0063, JAPAN

(ryuji, sone3)@yoyogi.ycc.u-tokai.ac.jp, (sdo, yoko)@keyaki.cc.u-tokai.ac.jp

^b Kokusai Kogyo Co., Ltd., 2-24-1 Harumi-cho, Fuchu, Tokyo 183-0057, JAPAN

(ryuji_matsuoka, naoki_shirai)@kkc.co.jp

Commission III, WG III/1

KEY WORDS: Analysis, Sampling, Measurement, Accuracy, Digital

ABSTRACT:

Our previous paper reported an experiment conducted in order to evaluate measurement methods of the center location of a circle by using simulated images of various sizes of circles. The variances of the measurement errors of the centroid methods in the experiment appeared to oscillate on a one-pixel cycle in diameter. This paper reports an analysis of the dependence of the measurement accuracy of the center location of a circle by the centroid methods on its diameter. Two centroid methods: intensity-weighted centroid method (WCM) and unweighted centroid method using a binary image created by thresholding (BCM) are investigated. Since general expressions representing the measurement accuracy by both WCM and BCM are unable to be obtained analytically, the variances of the measurement errors by both methods are obtained by numerical integration. From the results by the numerical integration, we conclude that sampling in digitization would cause the measurement accuracy of the center location of a circle by both WCM and BCM to oscillate on a one-pixel cycle in diameter. The results show that the variance of measurement errors by WCM can be expressed by the combination of the inverse proportion to the cube of the diameter and the oscillation on a one-pixel cycle in diameter. On the other hand, the variance of the measurement errors by BCM should approximate to the combination of the inverse proportion to the diameter and the oscillation on a one-pixel cycle in diameter.

1. INTRODUCTION

Circular targets are often utilized in photogrammetry, particularly in close range photogrammetry. Since a circle is radially symmetrical, circular targets are well suited for photogrammetric use such as camera calibration and 3D measurement. It is said that determination of the center of a circular target by digital image processing techniques is rotation-invariant and scale-invariant over a wide range of image resolutions. The center of a circular target can be estimated by centroid methods, by matching with a reference pattern, or by analytical determination of the circle center (Luhmann *et al.*, 2006).

Our previous paper (Matsuoka *et al.*, 2009) reported an experiment conducted in order to evaluate measurement methods of the center location of a circle by using simulated images of various sizes of circles. We investigated two centroid methods: intensity-weighted centroid method and unweighted centroid method using a binary image created by thresholding, and least squares matching in the experiment. We made the experiment by the Monte Carlo simulation using 1024 simulated images of which the centers were randomly distributed in one pixel for each circle. The radius of a circle was examined at 0.1 pixel intervals from 2 to 40 pixels. The variances of measurement errors by both centroid methods in the experiment appeared to oscillate on a 0.5 pixel cycle in radius, even though the formula to estimate the center of a circle by each centroid method does not seem to produce such cyclic measurement errors. We wondered whether the oscillation of the measurement accuracy by the centroid

methods might be caused by sampling in creating a digital image.

Bose and Amir (1990) reported the investigation of the effect of the shape and size of a square, a diamond, and a circle on the measurement accuracy of its center location by the unweighted centroid method using a binarized image. They conducted the analysis of the measurement accuracy of the center location of a square and showed the standard deviations of the measurement errors of the center location of a square derived from the variances of the measurement errors of the center location of a line segment. However, we confirmed that their study would be incomplete and the measurement accuracy of the center location of a square from 2 to 22 pixels in side shown in their paper is that when the side of a square is infinite. Moreover, they executed the simulation on the measurement accuracy of the center location of a circle. In their simulation, 400 binarized circles were placed at 0.05 pixel intervals covering a range of one pixel in x and y direction, and the radius of a circle was examined at merely 0.25 pixel intervals. Consequently, there was no mention finding cyclic measurement errors of the center location of a circle in their paper.

This paper reports an analysis of the dependence of the measurement accuracy of the center location of a circle by centroid methods on its diameter. Two centroid methods: intensity-weighted centroid method and unweighted centroid method using a binary image created by thresholding were investigated.

2. OUTLINE OF ANALYSIS

2.1 Process of Analysis

Since general expressions representing the measurement accuracy of the center location of a circle by the investigated centroid methods are unable to be obtained analytically, the variances of the measurement errors were obtained by numerical integration. We guessed that it was difficult to understand the characteristics of the measurement accuracy of the center location of a circle only by the results obtained by the numerical integration. Accordingly, we conducted the analyses of the measurement accuracy of the center location of a line segment and a square as well. We show the results of these analyses in advance.

2.2 Assumed Digital Image

In order to investigate the effects of sampling on the measurement accuracy of the center location of a figure, we assumed that images were sampled but not quantized in digitization. The gray value g_{ij} of the pixel (i, j) of an assumed digital image was the area of part of a figure inside the region $\{(x, y) \mid i \leq x \leq (i + 1), j \leq y \leq (j + 1)\}$. Therefore, $0 \leq g_{ij} \leq 1$. The image was assumed free of noise.

2.3 Measurement Methods

Centroid methods are relatively simple and theoretically independent of the image resolution. Furthermore, centroid methods do not require a template dependent on the image resolution. Accordingly, centroid methods are often utilized in measurement of the target location in photogrammetry.

We investigated two popular centroid methods. One was the intensity-weighted centroid method and is called WCM for short from now on. The other was the unweighted centroid method using a binary image created by thresholding and is called BCM for short from now on. While Hattori *et al.* (1999) adopted WCM in camera calibration, Chikatsu and Anai (2001) adopted BCM in camera calibration.

Although the standard deviation of the measurement errors by WCM would be theoretically proportional to the magnitude of image noises (Maas *et al.*, 1993), WCM would be expected to achieve the more accurate measurement for ordinary images. On the contrary, although BCM is robust against image noises, BCM would be unable to produce more accurate measurement results for ordinary images.

Both WCM and BCM estimate the center (x_c, y_c) of a figure by using the following equation (1):

$$\begin{cases} x_c = \frac{\sum_i \sum_j w_{ij} \cdot i}{\sum_i \sum_j w_{ij}} + \frac{1}{2} \\ y_c = \frac{\sum_i \sum_j w_{ij} \cdot j}{\sum_i \sum_j w_{ij}} + \frac{1}{2} \end{cases} \quad (1)$$

where, w_{ij} is the weight of the pixel (i, j) .

The difference between WCM and BCM is the difference of w_{ij} . While $w_{ij} = g_{ij}$ in WCM, $w_{ij} = 1$ if $g_{ij} \geq g_T$ and $w_{ij} = 0$ if $g_{ij} < g_T$ in BCM using the threshold g_T . We set g_T at the most ordinary value 1/2 in the analysis.

2.4 Numerical Integration

The variances of the measurement errors of the center location of a circle by both WCM and BCM and a square by BCM, which are unable to be obtained analytically, were obtained by numerical integration. Since the measurement errors of the center location of a circle by WCM are continuous versus the location of a figure, the variances of the measurement errors by WCM were obtained by the Simpson's rule. On the contrary, since measurement errors by BCM are not continuous versus the location of a figure, we obtained those variances by the midpoint rule. The size of a figure (the side of a square, the diameter of a circle) was examined at 1/128 pixel intervals from 2 to 20 pixels in the numerical integration.

2.5 Evaluation of Measurement Accuracy

All the averages of errors (ϵ_x, ϵ_y) in estimation of the center location of a line segment, a square, and a circle by WCM and BCM, which were obtained analytically or numerically, proved to be zero. The fact demonstrated that both WCM and BCM can estimate the center location of the figure without bias.

The measurement accuracy of the center location of a figure was measured by the variances (V_x, V_y) and $V (= V_x + V_y)$ of (ϵ_x, ϵ_y) . $V_x = V_y$, $V = 2V_x$, because both a square and a circle are point symmetry. We show a root mean squares of errors (RMSE) $\sqrt{V_x}$ of the center location of a line segment and \sqrt{V} of the center location of a square and a circle in the figures as well.

3. RESULTS AND DISCUSSION

3.1 Line Segment

It was assumed that a line segment with the length d was placed on the x -axis with its center on $(s + d/2, 0)$ ($0 \leq s < 1$).

The gray value g_i of the line segment is shown in Table 1. Here $\text{int}(x)$ and $\text{fra}(x)$ are the functions to return the integer and fractional parts of the value x respectively.

i	g_i
0	$(1 - s)$
$1 \leq i \leq \text{int}(s + d) - 1$	1
$\text{int}(s + d)$	$\text{fra}(s + d)$

Table 1. Grey value g_i of line segment

3.1.1 WCM: Equation (2) expresses the measurement error ϵ_x of the center location of the line segment by WCM derived from g_i shown in Table 1.

$$\epsilon_x = \frac{\{2(s + d) - \text{int}(s + d) - 1\} \text{int}(s + d)}{2d} + \frac{1}{2} - \left(s + \frac{d}{2}\right) \quad (2)$$

The variance V_x of ε_x can be obtained analytically and be expressed by Equation (3).

$$V_x = \frac{1}{12} \frac{\delta^2(1-\delta)^2}{d^2} \quad (3)$$

where δ is the fractional part of d , that is to say, $\delta = \text{fra}(d)$.

Equation (3) indicates that V_x oscillates on a one-pixel cycle in length and the local maxima of V_x in the one-pixel cycle are inversely proportional to the square of d . Moreover it shows that V_x has the local minima 0 in the one-pixel cycle when $\delta = 0$. Figure 1 shows the RMSE $\sqrt{V_x}$ from $d = 2$ to $d = 20$.

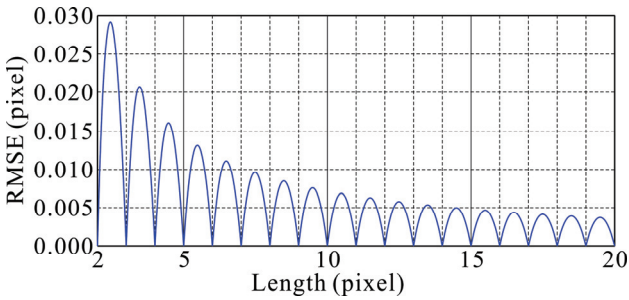


Figure 1. RMSE $\sqrt{V_x}$ of line segment by WCM

The result of the analysis demonstrates that sampling in digitization causes the measurement accuracy by WCM to oscillate on a one-pixel cycle in length.

3.1.2 BCM: Table 2 shows the measurement error ε_x of the center location of the line segment by BCM using the threshold $g_T = 1/2$ derived from g_i shown in Table 1. Here δ is the fractional part of d .

ε_x	$0 \leq \delta < \frac{1}{2}$	$\frac{1}{2} < \delta < 1$
$0 \leq s < \left(\frac{1}{2} - \delta\right)$	$-\left(s + \frac{\delta}{2}\right)$	$\frac{1}{2} - \left(s + \frac{\delta}{2}\right)$
$\left(\frac{1}{2} - \delta\right) \leq s \leq \frac{1}{2}$	$\frac{1}{2} - \left(s + \frac{\delta}{2}\right)$	
$\frac{1}{2} < s < \left(\frac{3}{2} - \delta\right)$	$1 - \left(s + \frac{\delta}{2}\right)$	$1 - \left(s + \frac{\delta}{2}\right)$
$\left(\frac{3}{2} - \delta\right) \leq s < 1$		$\frac{3}{2} - \left(s + \frac{\delta}{2}\right)$

$\delta = \text{fra}(d)$

Table 2. Measurement error ε_x of line segment by WCM

The variance V_x of ε_x can be obtained analytically and be expressed by Equation (4).

$$V_x = \frac{1}{4} \left\{ \left(\delta - \frac{1}{2} \right)^2 + \frac{1}{12} \right\} = \frac{1-3\delta(1-\delta)}{12} \quad (4)$$

Equation (4) indicates that V_x oscillates on a one-pixel cycle in length and is independent of the integer part of d . Figure 2 shows the RMSE $\sqrt{V_x}$ from $d = 2$ to $d = 5$.

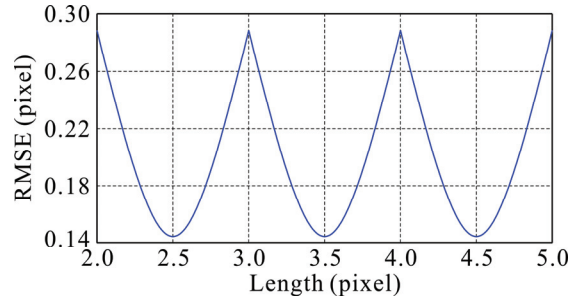


Figure 2. RMSE $\sqrt{V_x}$ of line segment by BCM

The result of the analysis demonstrates that sampling in digitization causes the measurement accuracy by BCM to oscillate on a one-pixel cycle in length as well as by WCM.

3.2 Square

It was assumed that a square with the side d was placed as each side was parallel to the x -axis or y -axis with its center on $(s + d/2, t + d/2)$ ($0 \leq s < 1, 0 \leq t < 1$).

The gray value g_{ij} of the square is shown in Table 3. Here $\text{int}(x)$ and $\text{fra}(x)$ are the functions to return the integer and fractional parts of the value x respectively.

g_{ij}	$i = 0$	$1 \leq i \leq (S - 1)$	$i = S$
$j = 0$	$(1 - s)(1 - t)$	$(1 - t)$	$s'(1 - t)$
$1 \leq j \leq (T - 1)$	$(1 - s)$	1	s'
$j = T$	$(1 - s)t'$	t'	$s't'$

$$S = \text{int}(s + d), T = \text{int}(t + d), s' = \text{fra}(s + d), t' = \text{fra}(t + d)$$

Table 3. Grey value g_{ij} of square

3.2.1 WCM: Equation (5) expresses the measurement error ($\varepsilon_x, \varepsilon_y$) of the center location of the square by WCM derived from g_{ij} shown in Table 3.

$$\left\{ \begin{array}{l} \varepsilon_x = \frac{\{2(s+d) - \text{int}(s+d) - 1\} \text{int}(s+d)}{2d} + \frac{1}{2} - \left(s + \frac{d}{2}\right) \\ \varepsilon_y = \frac{\{2(t+d) - \text{int}(t+d) - 1\} \text{int}(t+d)}{2d} + \frac{1}{2} - \left(t + \frac{d}{2}\right) \end{array} \right. \quad (5)$$

The variances (V_x, V_y) and V of ($\varepsilon_x, \varepsilon_y$) can be obtained analytically and be expressed by Equation (6).

$$\left\{ \begin{array}{l} V_x = V_y = \frac{1}{12} \frac{\delta^2(1-\delta)^2}{d^2} \\ V = V_x + V_y = 2V_x = \frac{1}{6} \frac{\delta^2(1-\delta)^2}{d^2} \end{array} \right. \quad (6)$$

where δ is the fractional part of d .

Equation (6) indicates that V oscillates on a one-pixel cycle in side similarly to V_x of the line segment with the length d and the local maxima of V in the one-pixel cycle are inversely proportional to the square of d . Moreover, it shows that V has the local minima 0 when $\delta = 0$ in the one-pixel cycle in the same way as V_x of the line segment. Figure 3 shows the RMSE \sqrt{V} from $d = 2$ to $d = 20$.

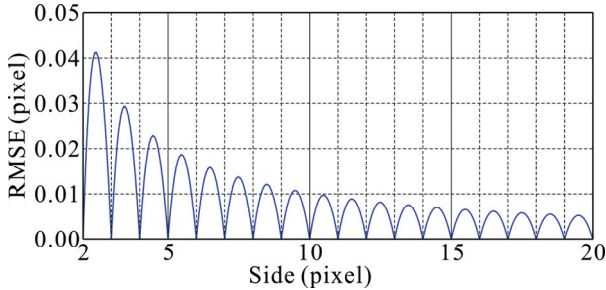


Figure 3. RMSE \sqrt{V} of square by WCM

The result of the analysis demonstrates that sampling in digitization causes the measurement accuracy by WCM to oscillate on a one-pixel cycle in side.

3.2.2 BCM: The region division of (s, t) according to the thresholding result of the pixel containing each vertex of the square is much complicated and it takes a large space to show the formulae of the measurement error $(\varepsilon_x, \varepsilon_y)$ of the center location of the square by BCM using the threshold $g_T = 1/2$. Furthermore, the variances (V_x, V_y) and V of $(\varepsilon_x, \varepsilon_y)$ are unable to be obtained analytically. Therefore, we decided to omit showing the formulae of $(\varepsilon_x, \varepsilon_y)$ in this paper.

V were obtained by numerical integration and Figure 3 shows the RMSE \sqrt{V} from $d = 2$ to $d = 20$.

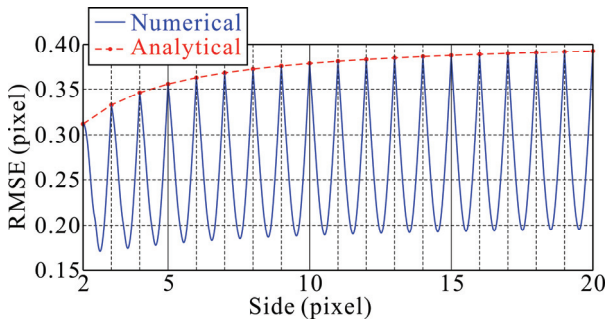


Figure 4. RMSE \sqrt{V} of square by BCM

The results by the numerical integration show that V oscillates on a one-pixel cycle in side similarly to V_x of the line segment. However, those show that the local maxima and local minima of V in the one-pixel cycle increase as d increases in contrast to the fact that V_x of the line segment is independent of the integer part of the length d . The increases of the local maxima and local minima of V with an increase in d could be explained in terms that the thresholding result of the pixel containing each vertex of the square would make the measurement accuracy higher and the influence of these four vertex pixels would decrease as d increases.

If $\delta = 0$, that is to say, d is an integer, V can be obtained analytically and be expressed by Equation (7). The red broken line in Figure 4 shows \sqrt{V} calculated by using Equation (7).

$$V = \left(-\frac{1}{2} + \log_e 2\right) \frac{1}{(d+1)^2} + \left(\frac{5}{2} - 4 \log_e 2\right) \frac{1}{(d+1)} + \frac{1}{6} \quad (7)$$

When $d \gg 1$, V becomes nearly independent of the integer part of d similarly to V_x of the line segment with the length d and could be approximated to Equation (8).

$$V = V_x + V_y = 2V_x = \frac{1-3\delta(1-\delta)}{6} \quad (8)$$

The results by the numerical integration show that sampling in digitization would cause the measurement accuracy by BCM to oscillate on a one-pixel cycle in side as well as by WCM.

3.3 Circle

It was assumed that a circle with the diameter d was placed as its center was located on $(s + d/2, t + d/2)$ ($0 \leq s < 1, 0 \leq t < 1$).

Table 4 shows the gray value g_{ij} of the circle when $d = 2$ and $t = 0$. The general expression of g_{ij} is complicated with sine and inverse sine functions in the same way as Table 4 shows. Consequently, the measurement error $(\varepsilon_x, \varepsilon_y)$ by either WCM or BCM is expressed by the combination of sine and inverse sine functions, and the variances (V_x, V_y) and V of $(\varepsilon_x, \varepsilon_y)$ are unable to be obtained analytically.

i	$g_{ij} (j=0, 1)$
0	$\left(\frac{\pi}{4} - \frac{1}{2}\theta_1\right) - \frac{1}{4}\sin 2\theta_1$
1	$\frac{1}{2}(\theta_1 + \theta_2) + \frac{1}{4}(\sin 2\theta_1 + \sin 2\theta_2)$
2	$\left(\frac{\pi}{4} - \frac{1}{2}\theta_2\right) - \frac{1}{4}\sin 2\theta_2$

$\theta_1 = \sin^{-1}(s), \theta_2 = \sin^{-1}(1-s)$

Table 4. Grey value g_{ij} of circle when $d = 2$ and $t = 0$

3.3.1 WCM: The variances (V_x, V_y) and V of the measurement errors $(\varepsilon_x, \varepsilon_y)$ of the center location of the circle by WCM were obtained by numerical integration. Figure 5 shows the RMSE \sqrt{V} from $d = 2$ to $d = 20$.

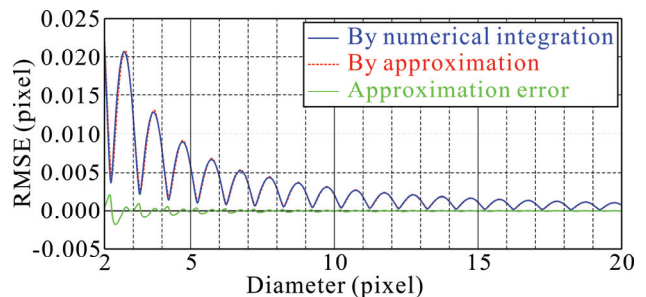


Figure 5. RMSE \sqrt{V} of circle by WCM

The results by the numerical integration show that V would oscillate on a one-pixel cycle in diameter similarly to V of the square with the side d . Those also show that V has the local maxima and local minima at $\delta \approx 3/4$ and $1/4$ in the one-pixel cycle respectively. Furthermore, those demonstrate that both the local maxima and local minima of V in the one-pixel cycle would be inversely proportional to the cube of d in contrast to the fact that the local maxima of V of the square with the side d are inversely proportional to the square of d . On the other hand, those indicate that V has the nonzero local minima in the one-pixel cycle contrary to V of the square with the side d .

Here ε_x when $d = 2$ and $t = 0$ can be obtained analytically and be expressed by Equation (9).

$$\varepsilon_x = \frac{1}{\pi} \left\{ \left(\theta_1 - \theta_2 + \frac{\pi}{2} \right) + \frac{1}{2} (\sin 2\theta_1 - \sin 2\theta_2) \right\} - s \quad (9)$$

where $\theta_1 = \sin^{-1}(s)$ and $\theta_2 = \sin^{-1}(1 - s)$. The fact that $\varepsilon_x \neq 0$ when $s \neq 0$ and $s \neq 1/2$ in Equation (9) suggests that V has the nonzero local minima in the one-pixel cycle.

It is assumed that V can be expressed in the similar formula to Equations (3) and (6) with the denominator of the cube of d . The approximation formula obtained by the least squares method using 2305 sets of (d, V) at $1/128$ pixel intervals from 2 to 20 pixels in d is as follows:

$$V_{\text{App.}} = \frac{0.008898 - 0.1388\delta_{1/4}^2(1 - \delta_{1/4})^2}{d^3} \quad (10)$$

where $\delta_{1/4}$ is the fractional part of $(\delta + 1/4)$, that is to say, $\delta_{1/4} = \text{fra}(\delta + 1/4)$.

The blue, red, and green lines in Figure 5 show \sqrt{V} by the numerical integration, $\sqrt{V_{\text{App.}}}$ by the approximation, and the approximation errors $(\sqrt{V_{\text{App.}}} - \sqrt{V})$ respectively. We studied the validity of the approximation formula (10) at $1/128$ pixel intervals from 2 to 100 pixels in d . The maximum absolute approximation error was 0.00203 pixel ($\sqrt{V} = 0.00536$, $\sqrt{V_{\text{App.}}} = 0.00739$) at $d = 2 + 23/128$. An absolute approximation error by Equation (10) is less than 0.0004 pixel when $d \geq 5$. Therefore, it can be concluded that the approximation formula (10) would be extremely effective.

The results by the numerical integration show that sampling in digitization would cause the measurement accuracy by WCM to oscillate on a one-pixel cycle in diameter.

3.3.2 BCM: The variances (V_x, V_y) and V of the measurement errors $(\varepsilon_x, \varepsilon_y)$ of the center location of the circle by BCM using the threshold $g_T = 1/2$ were obtained by numerical integration. Figure 6 shows the RMSE \sqrt{V} from $d = 2$ to $d = 20$.

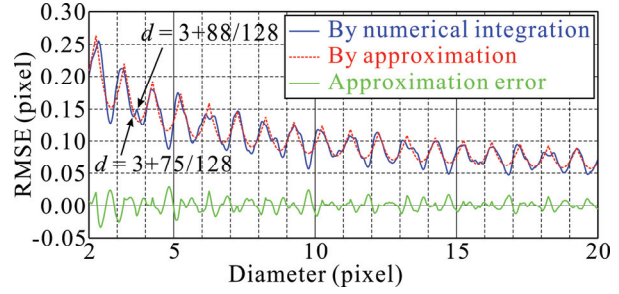


Figure 6. RMSE \sqrt{V} of circle by BCM

The results by the numerical integration show that V would oscillate on a one-pixel cycle in diameter similarly to V of the square with the side d . Those also show that V has the local maxima and local minima at $\delta \approx 1/4$ and $3/4$ in the one-pixel cycle respectively. Additionally those demonstrate that both the local maxima and local minima of V in the one-pixel cycle might be inversely proportional to d differently from V of the square with the side d .

While V of the square with the side d by BCM and V of the circle with the diameter d by WCM are smooth in the one-pixel cycle of d , V of the circle with the diameter d by BCM has small irregularities in the one-pixel cycle of d . As we guessed that the irregularities would be caused by the discontinuity of $(\varepsilon_x, \varepsilon_y)$, we studied distributions of $(\varepsilon_x, \varepsilon_y)$ at several values of d . Figure 7 shows the distributions of $\varepsilon = \sqrt{\varepsilon_x^2 + \varepsilon_y^2}$ at $d = 3 + 75/128$ and $d = 3 + 88/128$ where V has large irregularities in the one-pixel cycle of $3 \leq d \leq 4$. In order to compare with the distributions of ε of the circle show in Figure 7, Figure 8 shows the distributions of ε of the square with the side d at the same values of d as Figure 7. The larger $\varepsilon(i, j)$ is, the brighter (i, j) is in Figures 7 and 8.

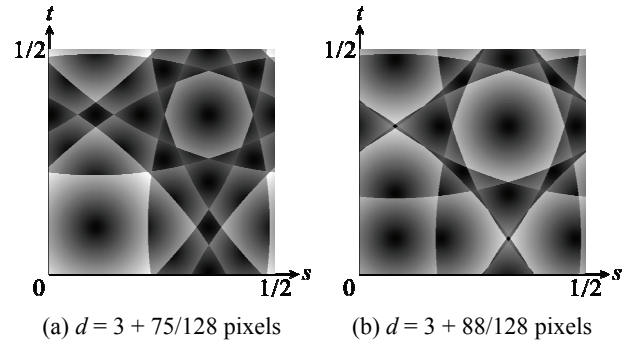


Figure 7. Measurement errors ε of circle by BCM

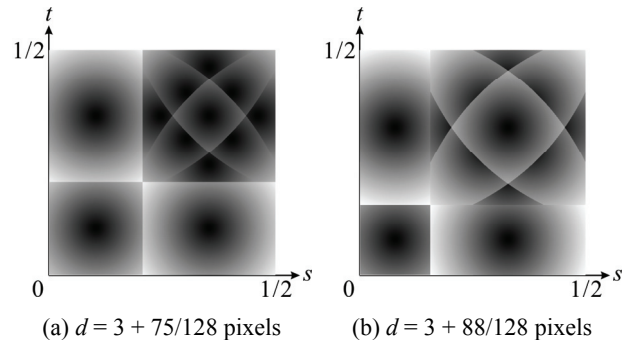


Figure 8. Measurement errors ε of square by BCM

The distributions of ε of the circle shown in Figure 7 are more complicated than those of ε of the square shown in Figure 8. Furthermore, although the difference of d between two distributions of ε of the circle shown in Figure 7 (a) and (b) is merely 13/128 pixel, two distributions would have a great difference in contrast to two distributions of ε of the square shown in Figure 8 (a) and (b). We concluded that the wide variation of the distribution of $(\varepsilon_x, \varepsilon_y)$ according to d would bring V having small irregularities of in the one-pixel cycle of d .

It is assumed that V can be expressed in the similar formula to Equation (4) with the denominator of d . The approximation formula obtained by the least squares method using 2305 sets of (d, V) at 1/128 pixel intervals from 2 to 20 pixels in d is as follows:

$$V_{\text{App.}} = \frac{0.15697 - 0.3706 \delta_{3/4} (1 - \delta_{3/4})}{d} \quad (11)$$

where $\delta_{3/4}$ is the fractional part of $(\delta + 3/4)$, that is to say, $\delta_{3/4} = \text{fra}(\delta + 3/4)$.

The blue, red, and green lines in Figure 6 show \sqrt{V} by the numerical integration, $\sqrt{V_{\text{App.}}}$ by the approximation, and the approximation errors $(\sqrt{V_{\text{App.}}} - \sqrt{V})$ respectively. We studied the validity of the approximation formula (11) at 1/128 pixel intervals from 2 to 100 pixels in d . The maximum absolute approximation error was 0.03312 pixel ($\sqrt{V} = 0.24281$, $\sqrt{V_{\text{App.}}} = 0.20969$) at $d = 2 + 53/128$. An absolute approximation error by Equation (11) is less than 0.025 pixel when $d \geq 5$ and less than 0.018 pixel when $d \geq 10$. The accuracy of the approximation (11) of V by BCM is obviously lower than that of the approximation (10) of V by WCM. The low accuracy of the approximation (11) would be caused by the wide variation of the distribution of $(\varepsilon_x, \varepsilon_y)$ according to d as mentioned previously. Nevertheless, we recognized that the approximation formula (11) is effective for ordinary use.

The results by the numerical integration show that sampling in digitization should cause the measurement accuracy by BCM to oscillate on a one-pixel cycle in diameter as well as by WCM.

4. CONCLUSIONS

Although general expressions representing the measurement accuracy of the center location of a circle by the two centroid methods WCM and BCM are unable to be obtained analytically, we succeeded in obtaining the variances of measurement errors by numerical integration and the effective approximation formulae of those. Additionally we conducted the analyses on the measurement accuracy of the center location of a line segment and a square by WCM and BCM.

From the results of these analyses, we concluded that sampling in creating a digital image would cause the measurement accuracy of the center location of a circle by both WCM and BCM to oscillate on a one-pixel cycle in diameter.

Moreover, we suggested that the variance of measurement errors by WCM is expressed by the combination of the inverse proportion to the cube of the diameter and the oscillation on a one-pixel cycle in diameter. On the other hand, the variance of measurement errors by BCM should approximate to the combination of the inverse proportion to the diameter and the oscillation on a one-pixel cycle in diameter.

We are planning to investigate the effect of quantization in creating a digital image on the measurement accuracy of the center location of a circle by both WCM and BCM. Furthermore, the influence of image noises on the measurement accuracy will be studied.

REFERENCES

- Bose, C.B., Amir, I., 1990. Design of Fiducials for Accurate Registration Using Machine Vision, *IEEE Transactions on Pattern Analysis and Machine Intelligence*, 12(12), pp. 1196-1200.
- Chikatsu, H., Anai, T., 2001. Development of Hybrid Video Theodolite System and Application to Image Sensing, *Journal of the Japan Society of Photogrammetry and Remote Sensing*, 40(1), pp. 31-42.
- Hattori, S., Akimoto, K., Okamoto, A., Hasegawa, H., Imoto, H., 1999. CCD Camera Calibration without Control Points by Multi-Photography of a Target Field, *IEICE Transactions on Information and Systems*, J82-D-II(9), pp. 1391-1400.
- Luhmann, T., Robson, S., Kyle, S., Harley, I., 2006. *Close Range Photogrammetry*, Whittles Publishing, Caithness, pp. 183-190.
- Maas, H.-G., Gruen, A., Papantoniou, D. A., 1993. Particle Tracking in three dimensional flows - Part I: Photogrammetric determination of particle coordinates, *Experiments in Fluids*, 15, pp. 133-146.
- Matsuoka, R., Sone, M., Sudo, N., Yokotsuka, H., Shirai, N., 2009. Comparison of Measuring Methods of Circular Target Location, *Journal of the Japan Society of Photogrammetry and Remote Sensing*, 48(3), pp. 154-170.